Spectral Method for Exploring Patterns of Diblock Copolymers

Kai Jiang[a], Yunqing Huang[a], Pingwen Zhang[*,b]

[a] *Hunan Key Laboratory for Computation and Simulation in Science and Engineering , Xiangtan University, P.R. China, 411105*
[b] *LMAM and School of Mathematical Sciences, Peking University, P.R. China, 100871*

Abstract

A numerical method in Fourier space is developed to solve the polymeric self-consistent field equations. The method does not require a priori symmetric information. More significantly, periodic structure can be adjusted automatically during the iteration process. In this article, we apply our method to diblock copolymer melt, thus reproduce all known stable phases, and reveal some meta-stable phases. It is worthy to point out that we also give an efficient strategy to estimating initial values for diblock copolymer system. Finally, by comparing with Matsen-Schick's method, we show some advantages of our method.

Key words: Self-consistent field theory; Diblock copolymer melt; Initial value; Phases; Matsen-Schick's method

1. Introduction

During the last decades, the various and fascinating ordered phases of block copolymer systems have been studied extensively [1, 2, 3]. The equilibrium morphology formed in periodically ordered state depends on compositions, interaction between distinct blocks, particular molecular architecture, and also the period structure. Theoretically, self-consistent field theory (SCFT) has proven itself to be a particularly successful framework for studying the phase behavior of block copolymers. It is a mean-field theory. By

[*]Corresponding author. Tel.: +86 10 6275 9851; fax: +86 10 6276 7146.
Email address: pzhang@pku.edu.cn. (Pingwen Zhang)
URL: http://www.math.pku.edu.cn/pzhang (Pingwen Zhang)

finding the solutions of SCFT equations, we can get the equilibrium order microstructures of block copolymers.

Due to the nonlinearity and the presence of multiple solutions, solving the SCFT analytically is a challenging problem. One successful approach is to apply numerical methods to solving the SCFT equations. It should be noted that the computational box can influence the final equilibrium morphologies [4]. Generally, the numerical methods can be classified into two categories. One type is calculated in Fourier space. Under an assumption of symmetry, Matsen and Schick [5] expanded the spatially varying functions in a finite set of basis functions, and obtained the first exact numerical phase diagram of three-dimensional ordered diblock copolymer phases. Then, based on this method, Tyler and Morse [6] minimized the SCFT free energy with respect to the computational box parameters according to a certain crystal system. Since this method assumes the symmetry and period structure of possible phases which determines the morphology of the solutions, it can not be used to discover new phases. Recently, Zhang and Zhang [7] have proposed an efficient numerical method based on Landau-Brazovsikii model. It does not require the assumption of the microphase symmetry, and the period structure can be adjusted automatically. Guo et al. [8] have proposed a generic Fourier space approach which does not need a priori knowledge of the structure of solutions and has been capable of discovering new equilibrium morphologies.

The other type is calculated in real space. A well known method called combinatorial screening algorithm was proposed by Drolet and Fredrickson [9]. The advantage of this method is that it does not require a priori assumption of symmetry, and can be used to discover new phases. A pseudospectral technology for solving the modified diffusion equation was introduced by Rasmussen and Kalosakas [10], which improves the computational efficiency of the real space methods. Based on density functional theory, Bohbot-Raviv and Wang [4] proposed a numerical method involving minimizing a free energy functional with respect to the composition profile and the size of the calculation area. For the real space methods, the calculation area is normally set as a cubic in 3D or a square in 2D, whereas the period of one ordered phase is not likely to be a cubic or a square. Thus the calculation area has to be set as large as possible, which significantly increases the computational complexity.

Solving the SCFT equations directly is unstable, thus several iteration methods have been devised for solving the self-consistent set of equations. In

the beginning, the nonlinear equation system methods have been chosen to update the field functions, such as Broyden method [5], Picard iteration [11] and Newton-Raphson method [6]. The disadvantage of these methods is that they have larger computational complexity. Then, a set of nonlinear optimization algorithms is introduced to solve SCFT equations. Drolet and Fredrickson [9] brought in a "simple mixing" iteration scheme, which has been proved to be usable, but slow and sometimes unstable [12]. To increase the stability, Tzeremes et al. [13] added density information into the "simple mixing" iteration scheme. To accelerate its convergence, Thompson et al. [12] proposed Anderson mixing, and Ceniceros et al. [14] introduced a class of semi-implicit methods and multilevel strategy.

Our research aims at developing a method in Fourier space that really doesn't need a priori symmetric information of basis functions, and the size and shape of the computational box can be adjusted automatically according to the period microstructures during the iteration process. The number of basis functions is decided by the given numerical accuracy. The numerical method based on Landau-Brazovsikii model [7] is the starting point of our study. The diblock copolymer melt has been extensively studied with SCFT [1, 3], so it is suitable for us to display our method. Because of the presence of multiple solutions of the nonlinear equation system, the solutions are sensitive to initial values. An appropriate method of estimating initial values is given to find the patterns quickly. Furthermore, we compare our approach with Matsen-Schick's method (MSM) [5, 6]. It is demonstrated that our method generates the same ordered phases as MSM, and the way to adjust the computational box in our method is not only more effective than that of MSM, but also more easily to reach the minimum value of free energy density in some cases. Meanwhile, the current method can be extended to other molecular architecture system.

The rest of the paper is organized as follows. In Section 2, we present the SCFT of diblock copolymer melt. In Section 3, we propose our numerical method. To verify the validity of our method, we report our numerical results and also compare it with MSM in Section 4. Finally, we give our conclusion in Section 5.

2. Self-consistence field theory

In this section, we will give a brief introduction to the self-consistent field theory of an incompressible diblock copolymer melt, more details can

be found in [2, 3, 5, 15]. We consider a system with volume V of n diblock copolymers each having A and B arms joined together with a covalent bond. The total degree of polymerization of a diblock copolymer is N, and the A-monomer fraction is f, correspondingly, the B-monomer fraction is $1-f$. The field-theoretic free energy density functional for the diblock copolymer melt is given by

$$h[\mu_+,\mu_-] = \frac{1}{V}\int d\mathbf{r}(-\mu_+ + \frac{1}{\chi N}\mu_-^2) - \log \mathcal{Q}[\mu_+,\mu_-]. \tag{1}$$

where χ is the Flory-Huggins segment-segment interaction parameter. $\mu_+(\mathbf{r})$ and $\mu_-(\mathbf{r})$ can be viewed as fluctuating pressure and exchange chemical potential fields, respectively. $\mathcal{Q}$ is the single-chain partition function, which is determined by

$$\mathcal{Q} = \frac{1}{V}\int d\mathbf{r}\, q(\mathbf{r},s), \qquad \forall s \in [0,1]. \tag{2}$$

The forward propagator $q(\mathbf{r},s)$ represents the probability density that the chain of contour length s has its end at position $\mathbf{r}$, where the variable s is used to parameter each copolymer chain, $s=0$ represents the tail of the A block and $s=f$ is the junction between the A and B blocks. Because $\mathcal{Q}$ is independent of s, we usually choose $\mathcal{Q} = (1/V)\int d\mathbf{r}\, q(\mathbf{r},1)$. From the standard Gaussian chain model [1, 3], we know that q satisfies the modified diffusion equation

$$\begin{aligned} \frac{\partial}{\partial s}q(\mathbf{r},s) &= R_g^2\nabla^2 q(\mathbf{r},s) - \omega(\mathbf{r},s)q(\mathbf{r},s), \\ q(\mathbf{r},0) &= 1, \end{aligned} \tag{3}$$

and

$$\omega(\mathbf{r},s) = \begin{cases} \omega_A(\mathbf{r}) = \mu_+(\mathbf{r}) - \mu_-(\mathbf{r}), & 0 \le s \le f, \\ \omega_B(\mathbf{r}) = \mu_+(\mathbf{r}) + \mu_-(\mathbf{r}), & f < s \le 1, \end{cases}$$

where $\omega_A(\mathbf{r})$, $\omega_B(\mathbf{r})$ are the external fields, which act on A and B monomers respectively, and R_g is the radius of gyration.

The normalized segment density operators in the sense of ensemble average ϕ_A and ϕ_B at $\mathbf{r}$ can be written as

$$\phi_A(\mathbf{r}) = \frac{1}{\mathcal{Q}}\int_0^f ds\, q(\mathbf{r},s)q^+(\mathbf{r},1-s), \tag{4}$$

$$\phi_B(\mathbf{r}) = \frac{1}{\mathcal{Q}}\int_f^1 ds\, q(\mathbf{r},s)q^+(\mathbf{r},1-s). \tag{5}$$

The reverse propagator, $q^+(\mathbf{r}, s)$, obeys (3) but ω satisfies

$$\omega(\mathbf{r}, s) = \begin{cases} \omega_B(\mathbf{r}), & 0 \le s \le 1-f, \\ \omega_A(\mathbf{r}), & 1-f < s \le 1. \end{cases}$$

Minimizing the free energy density functional with respect to the fields μ_+ and μ_-, we have SCFT equations

$$\frac{\delta h}{\delta \mu_+} = \phi_A(\mathbf{r}; \mu_\pm) + \phi_B(\mathbf{r}; \mu_\pm) - 1 = 0, \tag{6}$$

$$\frac{\delta h}{\delta \mu_-} = \phi_B(\mathbf{r}; \mu_\pm) - \phi_A(\mathbf{r}; \mu_\pm) + \frac{2\mu_-}{\chi N} = 0. \tag{7}$$

Our task is to find as many equilibrium states as possible by solving the SCFT equations.

3. Numerical method

As mentioned above, the computational box should be treated as variable in the method, therefore we need to add them to the spatially varying functions. Before doing this, a short introduction to the Bravais lattice and reciprocal lattice is necessary. The Bravais lattice is defined by $\mathbf{R}_l = l_1\mathbf{a}_1 + l_2\mathbf{a}_2 + l_3\mathbf{a}_3$, $l_1, l_2, l_3 \in \mathbf{Z}$, and the primitive vectors are denoted by $\mathbf{a}_1 = (a_{11}, a_{12}, a_{13})$, $\mathbf{a}_2 = (a_{21}, a_{22}, a_{23})$, $\mathbf{a}_3 = (a_{31}, a_{32}, a_{33})$. The corresponding reciprocal lattice primitive vectors are $\mathbf{b}_1 = (b_{11}, b_{12}, b_{13})$, $\mathbf{b}_2 = (b_{21}, b_{22}, b_{23})$, $\mathbf{b}_3 = (b_{31}, b_{32}, b_{33})$ and $\{\mathbf{G}\} = \{\mathbf{G}_{mnk} | \mathbf{G}_{mnk} = m\mathbf{b}_1 + n\mathbf{b}_2 + k\mathbf{b}_3\}$, where $m, n, k \in \mathbf{Z}$, are the reciprocal lattice. These two sets of primitive vectors satisfy $\mathbf{a}_i \cdot \mathbf{b}_j = 2\pi\delta_{ij}$, where $i, j = 1, 2, 3$. For brevity, element of $\{\mathbf{G}\}$ is sometimes written as $\mathbf{G}$ instead of $\mathbf{G}_{mnk}$, and $\mathcal{B} = (\mathbf{b}_1, \mathbf{b}_2, \mathbf{b}_3)$,

The equilibrium phases are periodic, free energy density functional depends not only on fields $\mu_\pm(\mathbf{r})$, composition, but also on the computational box. All spatially varying functions are periodic on the primitive lattice, and the plane waves $\{e^{i\mathbf{G}\cdot\mathbf{r}}\}$, $\mathbf{G} \in \{\mathbf{G}\}$, which form a basis for the function space $\{f(\mathbf{r} | f(\mathbf{r} + \mathbf{R}_l)) = f(\mathbf{r})\}$. The periodic function can be expanded as

$$f(\mathbf{r}) = \sum_{\{\mathbf{G}\}} f_{\mathbf{G}} e^{i\mathbf{G}\cdot\mathbf{r}}. \tag{8}$$

Thus all periodic functions are decided by the Fourier coefficients and reciprocal vectors $\mathcal{B}$.

Since for any $\mathbf{G}_1 + \mathbf{G}_2 + \cdots + \mathbf{G}_m \neq 0$, $m \in \mathbf{N}$, we have

$$\int_\Omega e^{i(\mathbf{G}_1+\mathbf{G}_2+\cdots+\mathbf{G}_m)\cdot\mathbf{r}} = 0, \tag{9}$$

the single-chain partition functional can be written as

$$\mathcal{Q} = \frac{1}{V}\int d\mathbf{r}\, q(\mathbf{r},1) = q_0(1), \tag{10}$$

and the free energy density functional h is

$$h[\mu_{\pm,\mathbf{G}};\mathcal{B}] = -\mu_{+,0} + \frac{1}{\chi N}\sum_{\mathbf{G}} \mu_{-,\mathbf{G}}\mu_{-,-\mathbf{G}} - \log q_0(1). \tag{11}$$

Eqs. (6) and (7) can be rewritten as

$$\frac{\delta h}{\delta \mu_{+,\mathbf{G}}} = \phi_{A,\mathbf{G}} + \phi_{B,\mathbf{G}} - \delta_{0,\mathbf{G}} = 0, \tag{12}$$

$$\frac{\delta h}{\delta \mu_{-,\mathbf{G}}} = \phi_{B,\mathbf{G}} - \phi_{A,\mathbf{G}} + \frac{2\mu_{-,\mathbf{G}}}{\chi N} = 0, \tag{13}$$

and Eqs. (4) and (5) turn to be

$$\phi_{A,\mathbf{G}} = \frac{1}{q_0(1)}\int_0^f ds \sum_{\mathbf{G}_1+\mathbf{G}_2=\mathbf{G}} q_{\mathbf{G}_1}(s)\, q^+_{\mathbf{G}_2}(1-s), \tag{14}$$

$$\phi_{B,\mathbf{G}} = \frac{1}{q_0(1)}\int_f^1 ds \sum_{\mathbf{G}_1+\mathbf{G}_2=\mathbf{G}} q_{\mathbf{G}_1}(s)\, q^+_{\mathbf{G}_2}(1-s). \tag{15}$$

The modified diffusion equation (3) is reduced to

$$\frac{dq_{\mathbf{G}}}{ds} = \begin{cases} \sum_{\mathbf{G}_1} A_{\mathbf{G}\mathbf{G}_1} q_{\mathbf{G}_1}(s), & 0 \le s \le f, \\ \sum_{\mathbf{G}_1} B_{\mathbf{G}\mathbf{G}_1} q_{\mathbf{G}_1}(s), & f < s \le 1, \end{cases} \tag{16}$$

where

$$A_{\mathbf{G}\mathbf{G}_1} = -R_g^2|\mathbf{G}|^2\delta_{\mathbf{G}\mathbf{G}_1} - \omega_{A,\mathbf{G}-\mathbf{G}_1},$$
$$B_{\mathbf{G}\mathbf{G}_1} = -R_g^2|\mathbf{G}|^2\delta_{\mathbf{G}\mathbf{G}_1} - \omega_{B,\mathbf{G}-\mathbf{G}_1}.$$

The initial condition is $q_G(0) = \delta_{G0}$. The Fourier coefficients q^+_G of reverse propagator satisfy the similar expression. In order to achieve the equilibrium

state, we require a set of Fourier coefficients $\{\mu_{\pm,\mathbf{G}}\}$ and primitive reciprocal vectors $\mathcal{B}$ that can minimize the free energy density. This can be separated into two problems.

1. Given $\mathcal{B}$, minimize the free energy density to find saddle-points $\{\mu_{\pm,\mathbf{G}}\}$;
2. Given a set of $\{\mu_{\pm,\mathbf{G}}\}$, find the reciprocal vectors of $\mathcal{B}$ to minimize the free energy density.

Both problems have to be solved simultaneously if $\{\mu_{\pm,\mathbf{G}}\}$ and $\mathcal{B}$ are solutions. In Sections 3.1 and 3.2, we will give the methods to solve the above two problems, respectively.

Theoretically, the set of basis functions is infinite. In practice, however, the spatially varying functions have to be expanded into finite basis functions, which means

$$f(\mathbf{r}) \approx f^{(N)}(\mathbf{r}) = \sum_{m,n,k} f(\mathbf{G}_{mnk}) e^{i\mathbf{G}_{mnk}\cdot\mathbf{r}}, \tag{17}$$

where $|m| \leq N$, $|n| \leq N$, $|k| \leq N$, and $m, n, k \in \mathbf{Z}$. In the expansion, the number of Fourier components is $(2N+1)^3$.

3.1. Given $\mathcal{B}$, find saddle-point $\mu_{\pm,\mathbf{G}}$

For diblock copolymer melt, an important fact is that the free energy density functional $h[\mu_\pm(\mathbf{r})]$ is to be maximized with respect to $\mu_+(\mathbf{r})$ and minimized with respect to $\mu_-(\mathbf{r})$ [3, 14]. Therefore, we choose the continuous steepest descent method to calculate saddle points without affecting the final results. More iteration methods can be found in [3, 9, 10, 13, 12, 14]. The continuous steepest descent method can be expressed as

$$\frac{\partial}{\partial s}\mu_+(\mathbf{r},s) = \lambda_+ \frac{\delta h[\mu_+,\mu_-]}{\delta \mu_+(\mathbf{r},s)}, \tag{18}$$

$$\frac{\partial}{\partial s}\mu_-(\mathbf{r},s) = -\lambda_- \frac{\delta h[\mu_+,\mu_-]}{\delta \mu_-(\mathbf{r},s)}, \tag{19}$$

where λ_+, $\lambda_- > 0$. Using explicit forward Euler scheme and Eqs. (12-13), we can obtain

$$\mu^{j+1}_{+,\mathbf{G}} = \mu^j_{+,\mathbf{G}} + \lambda_+ ds(\phi^j_{A,\mathbf{G}} + \phi^j_{B,\mathbf{G}} - \delta_{0,\mathbf{G}}), \tag{20}$$

$$\mu^{j+1}_{-,\mathbf{G}} = \mu^j_{-,\mathbf{G}} - \lambda_- ds\left(\phi^j_{B,\mathbf{G}} - \phi^j_{A,\mathbf{G}} + \frac{2\mu^j_{-,\mathbf{G}}}{\chi N}\right), \tag{21}$$

where $\phi^j_{A,\mathbf{G}}$, $\phi^j_{B,\mathbf{G}}$ can be calculated by Eqs. (14) and (15) through composite Simpson's rule. The pseudospectral technology, second-order operator-splitting scheme [10] was chosen to calculate $q_{\mathbf{G}}(s)$ and $q^+_{\mathbf{G}}(s)$.

When calculating $\phi_{A,\mathbf{G}}$ and $\phi_{B,\mathbf{G}}$, we use fast Fourier transform (FFT) to reduce the computational complexity. The key point is how to avoid the aliasing error in valuating the convolution sum $\sum_{\mathbf{G}_1+\mathbf{G}_2=\mathbf{G}} q_{\mathbf{G}_1}(s)\, q^+_{\mathbf{G}_2}(1-s)$. In our code, we use phase shift method to remove the error. The detail of the techniques can be found in [16].

3.2. Given $\mu_{\pm,\mathbf{G}}$, generate $\mathcal{B}$

If $\mathcal{B}$ is one of the solutions, the first derivatives of the free energy functional with respect to b_{mn} should be zero for $m, n = 1, 2, 3$. We can choose a proper coordinate system such that $b_{12} = 0$, $b_{13} = 0$, $b_{23} = 0$, $b_{11} \neq 0$, $b_{22} \neq 0$, $b_{33} \neq 0$. We update $\mathcal{B}$ through steepest descent method as

$$b^{j+1}_{mn} = b^j_{mn} - \alpha \frac{\partial h[\mathcal{B}]}{\partial b_{mn}}, \tag{22}$$

where $m, n = 1, 2, 3$, $m \leq n$. It is difficult to calculate $\partial h/\partial b_{mn}$ analytically, whereas we calculate it numerically. The value of α can be calculated by Armijo-Goldstein inexact line search algorithm [17]. Therefore, the size and shape of computational box can be automatically adjusted during the process of minimizing the free energy density.

Now, for a given N, we can obtain $\{\mu^{(N)}_{\pm,\mathbf{G}}\}$ and $\mathcal{B}$ according to the iteration process referred as Procedure I, which is specified in the following four steps.

Procedure I

Step 1 Given initial values $\{\mu_{\pm,\mathbf{G}}\}$, $\mathcal{B}$ and set $m = 1$, then calculate the free energy density h_m.

Step 2 Fixed $\mathcal{B}$, calculate $\{\mu_{\pm,\mathbf{G}}\}$ by the method described in Section 3.1.

Step 3 Adjust $\mathcal{B}$ and get the free energy density h_{m+1} by the method described in Section 3.2.

Step 4 Calculate the free energy density h_{m+1}, if $|h_{m+1} - h_m| > \varepsilon_1$, then set $h_m = h_{m+1}$, $m = m + 1$, go back to step 2.

3.3. The way to find appropriate N

Now, for a given N, we can calculate $\mu_{\pm,G}$ and $\mathcal{B}$ by Procedure I. However, spectral expansion $f^{(N)}$ is just an approximation of $f(\mathbf{r})$, we have the problem that how large is enough for N to make $f^{(N)}$ a good estimate of $f(\mathbf{r})$. If N is too large, the computational complexity may go beyond the computer's capacity; if N is too small, $f^{(N)}$ may be far away from $f(\mathbf{r})$. Getting the appropriate N within a tolerance is an adaptive process which is referred as Procedure II.

Procedure II

Step 1 Starting from a given N and reasonable initial values of $\mu^{(N)}_{\pm,\mathbf{G}}$, $\mathcal{B}^{(N)}$, apply Procedure I to generate $\mu^{(N)}_{\pm,\mathbf{G}}$, $\mathcal{B}^{(N)}$ and the free energy density value $h[\mu^{(N)}_{\pm,\mathbf{G}}; \mathcal{B}^{(N)}]$.

Step 2 Use $\mu^{(N)}_{\pm,\mathbf{G}}$ and $\mathcal{B}^{(N)}$ as the initial estimate of $N+k$ modes problem, and then apply Procedure I to generate $\mu^{(N+k)}_{\pm,\mathbf{G}}$, the corresponding $\mathcal{B}^{(N+k)}$, and the free energy density $h[\mu^{(N+k)}_{\pm,\mathbf{G}}; \mathcal{B}^{(N+k)}]$.

Step 3 Repeat the above step till

$$\left| h[\mu^{(N+k)}_{\pm,\mathbf{G}}; \mathcal{B}^{(N+k)}] - h[\mu^{(N)}_{\pm,\mathbf{G}}; \mathcal{B}^{(N)}] \right| < \varepsilon_2.$$

It means, the $(N+k)$, which makes the difference of the free energy density between N modes and $(N+k)$ modes less than a given small number ε_2, is the appropriate one. In practice, we set $k = 1$ and $\varepsilon_1 = \varepsilon_2 = 10^{-4}$.

3.4. The strategy to estimating good initial values

For Fourier space method, estimating initial values is to give the initial Fourier coefficients of $\mu_{-,G_{mnk}}$, while $\mu_{+,G_{mnk}}$ are all set as zero according to Eqs. (12-13). In other words, we should give the initial reciprocal vectors G_{mnk}, only on which the Fourier coefficients are nonzero. In the beginning, we set initial values randomly and executed our method repeatedly. The lamellar, cylinder phases usually appeared, whereas the complex structures such as gyroid, $Fddd$ phases seldom emerged. This implies that it is hard to find some required equilibrium states if we don't have any information about them because of the nonlinearity and the presence of multiple solutions. Some

authors [12, 18] also met the same problem. Therefore, choosing the suitable initial values should be investigated.

Generally, it is difficult for us to find the appropriate initial values for a nonlinear problem. Fortunately, the microscopic equilibrium state structures of the diblock copolymer melt demonstrate certain crystal symmetry. In the light of this fact we can obtain the initial reciprocal lattice vectors from Landau theory of block copolymers [19, 20, 21] or the crystal structure factor table [22]. The Landau theory of block copolymer is applied to weakly-segregated melts, and gives reciprocal lattice vectors that belong to different stable phases. Leiblei [19] has given these reciprocal lattice vectors of lamellar, hexagonal and body-centered cubic spheres (BCC) phases. The reciprocal lattice vectors of gyroid and face-centered cubic spheres (FCC) phases were given by Erukhimovich [20] and $Fddd$ phase has been studied by Ranjan et.al [21]. An alterative approach is directly using the crystal structure factor to obtain the reciprocal lattice vectors. However, this method does not tell us the main reciprocal lattice vectors required to expand the spatially varying functions initially. Maybe, we can use basis functions as many as possible in the beginning to depict the symmetry of ordered phases, but it brings more computational burden in adjusting the Fourier coefficients.

Table 1: The initial reciprocal vectors G_{mnk} of $\mu_{-,Gmnk}$ for BCC, FCC, gyroid and $Fddd$ phases.

Stable Phases	The initial reciprocal vectors G_{mnk}
BCC	$(01\bar{1})$, $(\bar{1}01)$, $(1\bar{1}0)$, $(0\bar{1}\bar{1})$, $(\bar{1}0\bar{1})$, $(\bar{1}\bar{1}0)$
FCC	(111), $(11\bar{1})$, $(1\bar{1}1)$, $(1\bar{1}\bar{1})$, (222), $(22\bar{2})$, $(2\bar{2}2)$, $(2\bar{2}\bar{2})$, (220), $(2\bar{2}0)$, (202), $(20\bar{2})$, (022), $(02\bar{2})$
Gyroid	$(\bar{2}11)$, $(\bar{2}\bar{1}\bar{1})^*$, $(21\bar{1})^*$, $(2\bar{1}1)$, $(1\bar{2}1)$, $(12\bar{1})$ $(\bar{1}\bar{2}\bar{1})^*$, $(\bar{1}21)^*$, $(11\bar{2})$, $(1\bar{1}2)^*$, $(\bar{1}12)$, $(\bar{1}\bar{1}\bar{2})$
$Fddd$	(111), $(11\bar{1})$, $(1\bar{1}1)$, $(1\bar{1}\bar{1})$, (220), $(2\bar{2}0)$, (004)

"*" denotes the sign of Fourier coefficients is opposite.

In this paper, we restrict our attention to the three-dimension stable phases, i.e. BCC, FCC, gyroid and $Fddd$. For these stable ordered phases, the initial reciprocal vectors of $\mu_{-,Gmnk}$ are summarized in Table 1. In view of centrosymmetry of these phases, we set $\mu_{-,G\bar{m}\bar{n}\bar{k}} = \mu_{-,Gmnk}$ at the same time. In Landau theory of block copolymer [20, 21], the reciprocal vectors of FCC phase are $\{111\}$ (including (111),$(11\bar{1})$, $(1\bar{1}1)$, $(1\bar{1}\bar{1})$), whereas from our experience, the final structure won't be the FCC phase if only the vectors

$\{111\}$ are used as initial ones. So we use crystal structure factor of $Fm\bar{3}m$ [22] to get the initial reciprocal vectors, as shown in Table 1. These estimating initial values are suitable to the weakly-segregated melt. Let the weakly-segregated results be the initial values, then the ordered phases at strong segregation can also be discovered. Of course, the approach of estimating initial values can be extended to real space method if we note Eq. (17).

From another point of view, the symmetric information has been used to estimate initial values. However, we don't change the essence feature of the method that it does not need a priori symmetry information of basis functions. The approximation space of our method is still the whole space. Our method can be used to discover new phases. Good initial values will help us accelerate the process to find the required solutions.

We will give some remarks on this numerical method. The similar numerical method has been applied to the Landau-Brazovsikii model by Zhang and Zhang [7]. However, it differs from ours. In Landau-Brazovsikii model, the free energy function is just a function of composition profile, and the first derivatives of the free energy function with respect to parameters of computational box can be calculated analytically. Meanwhile, the tactics to estimate initial values for diblock copolymer melt was not given in [7].

4. Numerical Results

4.1. Efficiency

The efficiency of our method will be shown in the following aspects: the stable phases can be captured; the computational box can be adjusted automatically and the meta-stable phases can also be discovered. The procedure II was run on Inter(R) Core(TM)2 Duo 2.66 GHz CPU with memory 2 G.

By applying these initial values above-mentioned and executing Procedure II, the different equilibrium stable phases can be discovered, as is shown in Fig. 1. The corresponding average time to convergence and the modes required are given in Table 2.

In order to show that the computational box can be adjusted automatically, we take gyriod phase calculated in an arbitrary box as an example. Other phases also have similar results. Fig. 2 shows the change tendency of the length of $\mathbf{a_1}$, $\mathbf{a_2}$, $\mathbf{a_3}$, the corresponding angles of θ_1, θ_2, θ_3. We can find that computational box converges to a cubic. The final morphology produced is shown in the third image from left in Fig. 1.

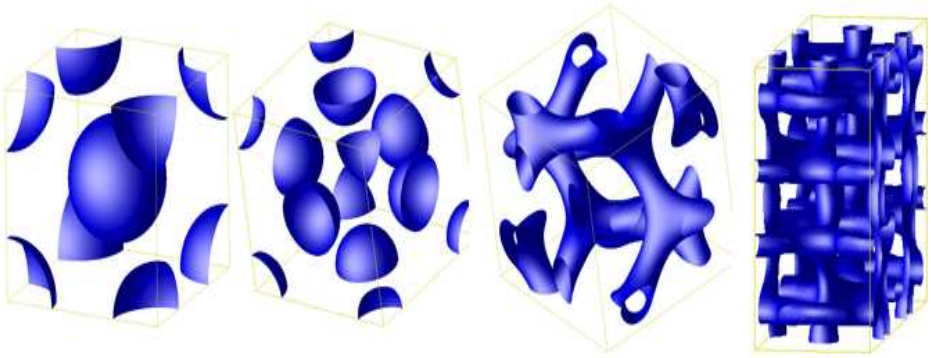

Figure 1: Stable phases, from left to right, BCC phase when $\chi N = 14.0$, $f = 0.3$; FCC phase when $\chi N = 17.67$, $f = 0.235$; gyroid phase when $\chi N = 14.0$, $f = 0.4$; $Fddd$ phase when $\chi N = 12.0$, $f = 0.43$, respectively.

Table 2: Modes required and CPU consuming of stable phases

	BCC	FCC	gyroid	$Fddd$
N	4	5	9	10
CPU time(s)	56	331	504	13378

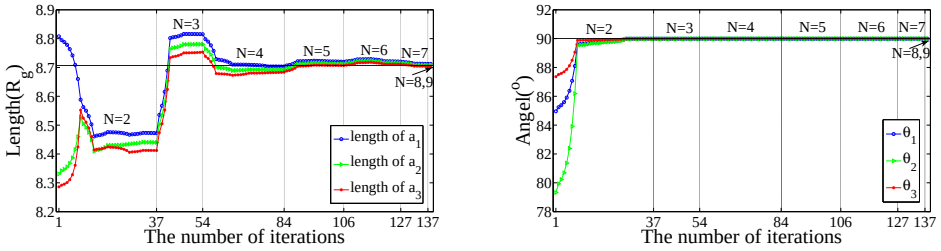

Figure 2: The adjustment of computational box during the iteration process.

We also discovered some meta-stable phases by inputting different initial values. By fixing coordinate $\chi N = 14.0$, $f = 0.4$ and applying our method, three meta-stable phases have been captured, as shown in Fig. 3. The left image in Fig. 3 shows BCC_3 phase as mentioned in [20]. A space group

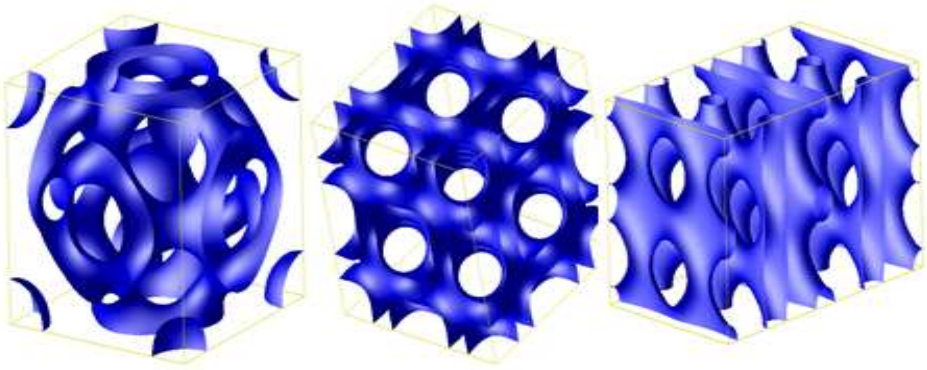

Figure 3: From left to right, three meta-stable phases BCC_3, $Fd\bar{3}m$ (space group symmetry) and perforated-lamellar phase when $\chi N = 14.0$, $f = 0.4$.

symmetry $Fd\bar{3}m$ phase is shown in the middle of Fig. 3. The right diagram in Fig. 3 shows perforated-lamellar phase.

4.2. Compare with Matsen-Schick's Method

Now we make some comparisons between Matsen-Schick's method (MSM) and our method (SMEP). Before that, we give a brief introduction to MSM.

4.2.1. An introduction to MSM

Here, we just address the differences in Fourier expansion from the standpoint of numerical computation. MSM is a Spectral-Galerkin method, more details can be found in [5, 6, 23]. The modified diffusion equation (3) is expanded as

$$\frac{dq_i}{ds} = \begin{cases} -R_g^2 \lambda_i D^{-2} q_i - \sum\limits_{j,k} \omega_{A,j} q_k \Gamma_{ijk}, & 0 \le s \le f, \\ -R_g^2 \lambda_i D^{-2} q_i - \sum\limits_{j,k} \omega_{B,j} q_k \Gamma_{ijk}, & f < s \le 1, \end{cases} \tag{23}$$

where $\Gamma_{ijk} = V^{-1} \int f_i(\mathbf{r}) f_j(\mathbf{r}) f_k(\mathbf{r}) d\mathbf{r}$, $f_i(r)$, $i = 1, 2, 3, ...$, are normalized orthonormal basis functions each possessing the symmetry of the phase obtained in [22], λ_i is the eigenvalues of the Laplacian operator: $\nabla^2 f_i(\mathbf{r}) = -\lambda_i D^{-2} f_i(\mathbf{r})$, and D is a length scale for the phase. The reverse propagator $q^+(\mathbf{r}, s)$ has the similar expression. The density operators (4-5) can be

written as

$$\phi_{A,i} = \frac{1}{q_0(1)} \int_0^f \sum_{j,k} q_j q_k \Gamma_{ijk}, \tag{24}$$

$$\phi_{B,i} = \frac{1}{q_0(1)} \int_f^1 \sum_{j,k} q_j q_k \Gamma_{ijk}, \tag{25}$$

It should be noted that the FFT technology can not be used to solve modified diffusion equations (23) and density functions (24-25) due to the special basis functions.

In the following, the same iteration process as described in Section 3 was used for MSM including adjustment of the computational box. However, the number of computational box parameters to be adjusted depends on the crystal system, e.g., the length of the side of a cubic crystal, the length of the three orthogonal edges of an orthorhombic crystal, or the three angles and three lengths of a triclinic crystal [6]. It differs from SMEP that all the parameters of computational box can be adjusted freely during the iteration process.

4.2.2. Comparison results

In the section, we will compare the results of the two type of spectral methods. We focus our attention on BCC and gyroid phases. Because BCC and gyroid phases both belong to cubic crystal system, only the length of any one edge of cubic is adjusted in MSM. In order to compare the two numerical methods, the same initial conditions. For MSM, the reciprocal vectors (110) and (211) were set as the initial vectors for BCC phase and gyroid phase, respectively. The initial reciprocal vectors for SMEP were given in Table 1. The cubic with length of edge $4.45R_g$ and length of edge $8.7R_g$ were set as the initial computational box for BCC and gyroid phases, respectively, for both methods. The error tolerance, ε_1 and ε_2, of these two methods were both set as 10^{-4}. In calculation, we fixed the coordinates at $\chi N = 14.0$, $f = 0.3$ for BCC phase and $\chi N = 14.0$, $f = 0.4$ for gyroid phase.

After executing Procedure II, we can obtain the similar images, BCC and gyroid phases, as shown in Fig. 1 by two methods. The computational box converges to a cubic in SMEP. A more detailed comparison is mapping the Fourier coefficients calculated by SMEP to those corresponding the Bragg reflections of morphology [22]. We found that the ordered phases, BCC and gyroid phases, obtained by SMEP belong to corresponding space group,

Table 3: The magnitude of nonzero Fourier coefficients $\phi_{A,G_{mnk}}$ for BCC and gyroid phases obtained by MSM and SMEP. The index of reciprocal vector (mnk) includes reciprocal vectors within a star of point group symmetry $m\bar{3}m$ both for BCC and gyroid phases.

BCC				Gyroid			
(mnk)	MSM	SMEP	Difference	(mnk)	MSM	SMEP	Difference
(000)	0.30000	0.30000	0.00000	(000)	0.40000	0.40000	0.00000
(110)	0.03307	0.03291	0.00016	(211)	0.05373	0.05371	0.00002
(200)	0.00939	0.00932	0.00007	(220)	0.02609	0.02590	0.00019
(211)	0.00225	0.00223	0.00002	(444)	0.00253	0.00248	0.00005
(222)	0.00045	0.00045	0.00000	(611)	0.00203	0.00203	0.00000
(321)	0.00036	0.00036	0.00000	(400)	0.00184	0.00187	0.00003
(310)	0.00036	0.00036	0.00000	(543)	0.00170	0.00166	0.00004
(220)	0.00026	0.00025	0.00001	(440)	0.00142	0.00145	0.00003
(400)	0.00025	0.00023	0.00002	(321)	0.00140	0.00140	0.00000
(330)	0.00018	0.00018	0.00000	(631)	0.00123	0.00122	0.00001
(411)	0.00018	0.00017	0.00001	(541)	0.00120	0.00118	0.00002
...	...	...	...	...	...	...	...

$Im\bar{3}m$ and $Ia\bar{3}d$, respectively. The result is also consistent with Guo et.al [8]. The deviation of Fourier coefficients of $\phi_{A,G_{mnk}}$ between MSM and SMEP for BCC and gyroid phases is shown in Table 3. The index of reciprocal vector (mnk) in Table 3 indicates that the reciprocal vectors is within a star of point group symmetry $m\bar{3}m$ both for BCC and gyroid phases. Therefore, MSM and SMEP can calculate the same ordered phases with delicate difference in Fourier coefficients.

Table 4: Comparison of free energy density and length of edge

	BCC		gyroid	
	MSM	SMEP	MSM	SMEP
Energy density	-0.561042	-0.561619	-0.266687	-0.269220
Length of edge	4.520909	4.516176	8.726663	8.708911

Table 4 shows the eventually convergent results: the free energy density and the length of the edge of computational box. From Table 4, we observe that the free energy density obtained by SMEP is lower than that of MSM. It might be related with the Fourier coefficients and the computational box. The derivation in Fourier coefficients between MSM and SMEP is small, similarly as shown in Table 3. Therefore, the most possible reason is the

difference of computational box, which is also mentioned in [4, 6]. SMEP can make free energy density converge to its minimum value easily.

Table 5: The iterations of Procedure I required for various N.

	BCC			gyroid	
N	MSM	SMEP	N	MSM	SMEP
1	**	3			
2	23	3	2	2	5
3	3	2	3	51	3
4	1	1	4	9	4
			5	**	3
			6	**	3
			7	6	2
			8	14	2
			9	1	1

"**" means that the iterations is more than 200.

Table 5 shows the number of iterations required of Procedure I, including finding the saddle points of $\mu_{\pm}$ and adjusting the computational box. In Table 5, we find the method to adjust computational box in SMEP is more effective than that of MSM according to the number of iterations of Procedure I. The optimization algorithm of adjusting the computational box may also affect the number of iterations.

Table 6: The principal relationship between numbers of basis functions of MSM and SMEP

	BCC	FCC	gyroid	$Fddd$
N_m	$N_x/96$	$N_x/64$	$N_x/96$	$N_x/16$

Then, we will give a rough computational complexity analysis. When the mode number increases to N, the number of Fourier coefficients of SMEP is $N_x \sim O((2N+1)^3)$. The computational effort to calculate Eqs. (14-16) in SMEP is $O(N_s N_x log N_x)$, where N_s is the number of chain contour steps. The number of basis functions of MSM, N_m, is determined by the symmetry and Bravais lattice of a certain space group [22]. The principal relationship

between numbers of basis functions of two methods is shown in Table 6. However, the computational effort of MSM to calculate Eqs. (23-25) is $O(N_s N_m^2)$. Therefore, when calculating the modified diffusion equation and density operations, for BCC and gyroid phases, the computational complexity of MSM is larger than that of SMEP when the modes N is greater than 23. The conclusion holds when N is greater than 18 for FCC phase or 6 for $Fddd$. However, the final computational complexity is heavily dependent on the iteration method for updating the field functions and the way to adjust the computational box.

From MSM and SMEP, we can obtain the same ordered structures that belong to the corresponding space group for diblock copolymer melt. The way to adjust the computational box by SMEP removes the constraints of the size and shape of computational box, which makes the free energy achieve its minimum value easily and more effective than that of MSM. In strongly-segregated system, a large number of basis functions are required for capturing the sharp interface [15]. SMEP can reduce the computational complexity with the FFT technology. SMEP can also relieve the programmers' burden because all phases can be calculated by the same code, while MSM need different codes for different phases. Meanwhile, for more complex copolymers, SMEP can be extended to other topological architecture easily because the symmetrical information is not required.

5. Conclusion

A novel numerical method, which does not need a priori symmetric information and can adjust the period structure automatically, is developed based on SCFT. Here, the method is applied to diblock copolymer system. Ever though the SCFT equations are nonlinear system and exist the multiple solutions, an efficient method for estimating initial values is given in the light of symmetrical microstructures of diblock copolymer system. Using the method, we calculated all stable phases of diblock copolymers discovered in the experiment, FCC, BCC, cylinder, gyroid, lamellar and $Fddd$ phases and also captured some metastable phases. We also compared our method with Matsen-Schick's method. Numerical examples demonstrate that our method has some advantages over MSM. Our future work is to apply the current method to other block copolymer systems based on SCFT as well.

Acknowledgements

The authors would like to acknowledge Prof. An-Chang Shi for the help on understanding the MSM; X.W. Zhang, W.Q. Xu and X.Y. Cheng for their useful suggestions. P.W. Zhang would like to thank the financial support by the special funds for Major State Research Projects (2005CB321704), and National Natural Science Foundation of China (50930003). Y.Q. Huang is supported by the NSFC for Distinguished Young Scholars under Grant 10625106 and National Basic Research Program of China under Grant 2005CB321701. K. Jiang is supported by Visit Project For Postgraduate of Peking University and Hunan Provincial Innovation Foundation For Postgraduate (CX2009B118).

References

[1] M.W. Matsen, The standard Gaussian model for block copolymer melts, J. Phys.: Condens. Matter 14 (2002) R21-R47.

[2] G.H. Fredrickson, V. Ganesan, F. Drolet, Field-theoretic computer simulation methods for polymers and complex fluids, Macromolecules 35 (2002) 16.

[3] G.H. Fredrickson, The Equilibrium Theory of Inhomogeneous Polymers, Oxford Press, 2006.

[4] Y. Bohbot-Raviv, Z.G. Wang, Discovering new ordered phases of block copolymers, Phys. Rev. Lett. 85 (2000) 3428.

[5] M.W. Matsen, M. Schick, Stable and unstable phases of a diblock copolymer melt, Phys. Rev. Lett. 72 (1994) 2660.

[6] C.A. Tyler, D.C. Morse, Stress in self-consistent-field theory, Macromolecules 36 (2003) 8184.

[7] P.W. Zhang, X.W. Zhang, An efficient numerical method of Landau-Brazovsikii model, J. Comp. Phys. 227 (2008) 5859.

[8] Z.J. Gou, G.J. Zhang, F. Qiu, H.D. Zhang, Y.L. Yang, A.C. Shi, Discovering ordered phases of block copolymers: new results from a generic Fourier-Space approach, Phys. Rev. Lett. 101 (2008) 28301.

[9] F. Drolet, G.H. Fredrickson, Combinatorial screening of complex block copolymer assembly with self-consistent field theory, Phys. Rev. Lett. 83 (1999) 4317.

[10] K.Ø. Rasmussen, G. Kalosakas, Improved numerical algorithm for exploring block copolymer mesophases, J. Polymer Science Part B-Polymer Physics 40 (2002) 1777.

[11] A.C. Shi, J. Noolandi, R.C. Desai, Theory of anisotropic fluctuations in ordered block copolymer phases, Macromolecules 29 (1996) 6487.

[12] R.B. Thompson, K.Ø. Rasmussen, T. Lookman, Improved convergence in block copolymer self-consistent field theory by Anderson mixing, J. Chem. Phys. 120 (2004) 31.

[13] G. Tzeremes, K.Ø. Rasmussen, T. Lookman, A. Saxena, Efficient computation of the structural phase behavior of block copolymers, Phys. Rev. E 65 (2002) 41806.

[14] H.D. Ceniceros, G.H. Fredrickson, Numerical solution of polymer self-consistent field theory, Multiscale Model. Simul. 2 (2004) 452.

[15] E.W. Cochran, C.J. Garcia-Cervera, G.H. Fredrickson, Stability of the gyroid phase in diblock copolymers at strong segregation, Macromolecules 39 (2006) 2449.

[16] C.G. Canuto, M.Y. Hussaini, A. Quarteroni, T.A. Zang, Spectral Methods in Fluid Dynamics, Springer-Verlag, 1988.

[17] J. Nocedal, S.J. Wright, Numerical Optimization, Springer, 2000.

[18] J.Z. Chen, C.X. Zhang, Z.Y. Sun, Y.S. Zheng, L.J. An, A novel self-consistent-field lattice model for block copolymers, J. Chem. Phys. 124 (2006) 104907.

[19] L. Leibler, Theory of microphase separation in block copolymers, Macromolecules 13 (1980) 1602.

[20] I.Y. Erukhimovich, Weak segregation theory and non-conventional morphologies in the ternary ABC triblock copolymers, Eur. Phys. J. E 18 (2005) 383.

[21] A. Ranjan, D.C. Morse, Landau theory of the orthorhombic $Fddd$ phase, Phys. Rev. E 74 (2006) 11803.

[22] N.F.M. Henry, K. Lonsdale, International tables for X-ray crystallography, Kynoch Press, 1952.

[23] A.C. Shi, Developments in Block Copolymer Science and Technology, edited by I. Hamley, Wiley, 2004.